Monthly Notices
of the
ROYAL ASTRONOMICAL SOCIETY

Mon. Not. R. Astron. Soc. **425,** 2116–2127 (2012) doi:10.1111/j.1365-2966.2012.21524.x

The Arizona CDFS Environment Survey (ACES): A Magellan/IMACS Spectroscopic Survey of the *Chandra Deep Field*-South★

Michael C. Cooper,[1,2]†‡§ Renbin Yan,[3] Mark Dickinson,[4] Stéphanie Juneau,[2,5] Jennifer M. Lotz,[6] Jeffrey A. Newman,[7] Casey Papovich,[8] Samir Salim,[9] Gregory Walth,[2] Benjamin J. Weiner[2] and Christopher N. A. Willmer[2]

[1]*Center for Galaxy Evolution, Department of Physics and Astronomy, University of California, Irvine, 4129 Frederick Reines Hall, Irvine, CA 92697, USA*
[2]*Steward Observatory, University of Arizona, 933 North Cherry Avenue, Tucson, AZ 85721, USA*
[3]*Department of Physics and Astronomy, University of Kentucky, Lexington, KY 40506, USA*
[4]*National Optical Astronomy Observatory, 950 North Cherry Avenue, Tucson, AZ 85719, USA*
[5]*Laboratoire AIM, CEA/DSM-CNRS-Université Paris Diderot, Irfu/Service dAstrophysique, CEA-Saclay, Orme des Merisiers, 91191 Gif-sur-Yvette Cedex, France*
[6]*Space Telescope Science Institute, 3700 San Martin Drive, Baltimore, MD 21218, USA*
[7]*Department of Physics and Astronomy and Pittsburgh Particle Physics, Astrophysics, and Cosmology Center (PITT-PACC), University of Pittsburgh, 3941 O'Hara Street, Pittsburgh, PA 15260, USA*
[8]*Department of Physics and Astronomy, Texas A&M University, College Station, TX 77845, USA*
[9]*Department of Astronomy, Indiana University, Bloomington, IN 47404, USA*

Accepted 2012 June 14. Received 2012 June 2; in original form 2011 December 1

ABSTRACT

We present the Arizona CDFS Environment Survey (ACES), a recently completed spectroscopic redshift survey of the Chandra Deep Field-South (CDFS) conducted using the Inamori-Magellan Areal Camera and Spectrograph on the Magellan-Baade telescope. In total, the survey targeted 7277 unique sources down to a limiting magnitude of $R_{\rm AB} = 24.1$, yielding 5080 secure redshifts across the ∼30 arcmin × 30 arcmin extended CDFS region. The ACES data set delivers a significant increase to both the spatial coverage and the sampling density of the spectroscopic observations in the field. Combined with previously published spectroscopic redshifts, ACES now creates a highly complete survey of the galaxy population at $R < 23$, enabling the local galaxy density (or environment) on relatively small scales (∼1 Mpc) to be measured at $z < 1$ in one of the most heavily studied and data-rich fields in the sky. Here, we describe the motivation, design and implementation of the survey and present a preliminary redshift and environment catalogue. In addition, we utilize the ACES spectroscopic redshift catalogue to assess the quality of photometric redshifts from both the COMBO-17 and Multiwavelength Survey by Yale-Chile imaging surveys of the CDFS.

Key words: catalogues – surveys – galaxies: distances and redshifts.

1 INTRODUCTION

Building upon the initial X-ray observations of Giacconi et al. (2001, 2002), the *Chandra Deep Field*-South (CDFS; $\alpha = 03^{\rm h}32^{\rm m}25^{\rm s}$, $\delta = -27^{\circ}49'58''$) has quickly become one of the most well-studied extragalactic fields in the sky with existing observations among the deepest at a broad range of wavelengths (e.g. Giavalisco et al. 2004; Rix et al. 2004; Lehmer et al. 2005; Quadri et al. 2007; Miller et al. 2008; Padovani et al. 2009; Cardamone et al. 2010; Damen et al. 2011; Xue et al. 2011; Elbaz et al., in preparation). In the coming years, this status as one of the very deepest multiwavelength survey fields will be further cemented by the ongoing and upcoming extremely deep observations with *Spitzer*/IRAC and *Hubble Space Telescope* (*HST*)/WFC3-IR as part of the Spitzer Extended Deep Survey (SEDS, PI: G. Fazio) and the Cosmic Assembly Near-infrared Deep Extragalactic Legacy Survey (CANDELS; Grogin et al. 2011; Koekemoer et al. 2011), respectively.

Despite the large commitment of telescope time from both space- and ground-based facilities devoted to imaging the CDFS,

★ This paper includes data gathered with the 6.5 m Magellan Telescopes located at Las Campanas Observatory, Chile.
†E-mail: m.cooper@uci.edu
‡*Hubble* Fellow.
§*Spitzer* Fellow.

spectroscopic observations in the field have generally lagged those in other comparably deep extragalactic survey fields. For example, in the Extended Groth Strip (EGS), another deep field targeted by the SEDS and CANDELS programmes, the DEEP2 and DEEP3 Galaxy Redshift Surveys (Davis et al. 2003, 2007; Cooper et al. 2011, 2012b; Newman et al. 2012; Cooper et al., in preparation; see also Weiner et al. 2006) have created a vast spectroscopic data base, achieving an impressive ∼60 per cent redshift completeness down to $R_{\rm AB} = 24.1$ across more than 0.2 square degrees and $\gtrsim$40 per cent completeness covering a broader area of ∼0.5 square degrees down to the same magnitude limit. Similarly, there have been a variety of spectroscopic efforts in the GOODS-N field including the Team Keck Redshift Survey (TKRS; Wirth et al. 2004, see also Cooper et al. 2011) in addition to the independent work of various groups (e.g. Lowenthal et al. 1997; Phillips et al. 1997; Cohen et al. 2000; Dawson et al. 2001; Cowie et al. 2004; Treu et al. 2005; Reddy et al. 2006; Barger, Cowie & Wang 2008). Together, these data sets provide spectroscopic redshifts for >90 per cent of sources down to $z_{\rm F850LP} = 23.3$ (Barger et al. 2008).

These large spectroscopic surveys add significant scientific utility to the associated imaging data sets, making the photometric constraints much more powerful. For example, spectroscopic redshifts allow critical rest-frame quantities to be derived with increased precision. Furthermore, only through spectroscopy can assorted spectral and dynamical properties (such as the strengths and velocity widths of emission and absorption lines) be measured – in this regard, the spectral data bases provided by surveys such as DEEP2, DEEP3 and TKRS are especially powerful due to their uniform spectral range and resolution. Finally, only with the combination of high (and relatively uniform) sampling density, spatial coverage across a modestly sized field (e.g. $\gtrsim$0.05 square degrees) and moderately high-precision spectroscopic redshifts (i.e. $\sigma_z < 0.01$) can the local galaxy density (or 'environment') be measured across a broad and continuous range of environments (Cooper et al. 2005, 2007).

In contrast to the EGS and GOODS-N fields, the spectroscopic redshift completeness across the extended 30 arcmin × 30 arcmin area of the CDFS is modest, $\lesssim$25 per cent down to a limiting magnitude of $R_{\rm AB} = 23$ and $\lesssim$20 per cent at $R_{\rm AB} < 24$, despite some significant spectroscopic efforts in the field (e.g. Le Fèvre et al. 2004; Szokoly et al. 2004; Mignoli et al. 2005; Vanzella et al. 2005, 2006, 2008; Ravikumar et al. 2007; Popesso et al. 2009; Balestra et al. 2010; Silverman et al. 2010).[1] Notably, many of these existing spectroscopic programmes have focused their efforts on the smaller GOODS-S region and/or targeted optically faint, higher redshift ($z > 1.5$) sources (e.g. Dickinson et al. 2004; Doherty et al. 2005; Roche et al. 2006; Vanzella et al. 2009).

With the goal of creating a highly complete redshift survey at $z < 1$ in the CDFS, the Arizona CDFS Environment Survey (ACES) utilized the Inamori-Magellan Areal Camera and Spectrograph (IMACS; Dressler et al. 2011) on the Magellan-Baade telescope to collect spectra of more than 7000 unique sources across an ∼30 arcmin × 30 arcmin region centred on the CDFS. In Sections 2 and 3, we describe the design, execution and reduction of the ACES observations, with a preliminary redshift and environment catalogue presented in Sections 4 and 5. Finally, in Section 6, we conclude with a discussion of future work related to ACES. Throughout, we employ a Lambda cold dark matter cosmology with $w = -1$, $\Omega_{\rm m} = 0.3$, $\Omega_\Lambda = 0.7$ and a Hubble parameter of $H_0 = 100\,h\,{\rm km\,s^{-1}\,Mpc^{-1}}$. All magnitudes are on the AB system (Oke & Gunn 1983), unless otherwise noted.

2 TARGET SELECTION AND SLITMASK DESIGN

The ACES target sample is drawn from the COMBO-17 photometric catalogue of Wolf et al. (2004, see also Wolf et al. 2001, 2008). The primary spectroscopic sample is magnitude limited at $R_{\rm AB} < 23$, plus a significant population of fainter sources down to $R_{\rm AB} = 24.1$. Altogether, ACES observations spanned four separate observing seasons (2007B–2010B), with the details of the target-selection algorithm and slitmask design parameters varying from year to year. Here, we highlight the critical elements of the composite target population and slitmasks, including any significant variations from mask to mask.

As stated above, the primary target sample for ACES was selected according to an R-band magnitude limit of $R_{\rm AB} < 23$. Selecting in R (versus a redder passband such as I or K) ensures the highest possible signal-to-noise ratio in the continuum of the resulting optical spectra, and thus a high redshift-success rate for the survey. The given magnitude limit was adopted to enable a high level of completeness to be reached across the entire CDFS area. Moreover, at $z \sim 1$, the $R = 23$ limit reaches L^* along the red sequence and 1 mag fainter than L^* in the blue cloud population (Willmer et al. 2006), thereby enabling ACES to probe the systems that dominate the galaxy luminosity density and global star formation rate at $z < 1$. As shown in Fig. 1, ACES is highly complete at $R < 23$, achieving a targeting rate of $\gtrsim$80 per cent across the extended CDFS.

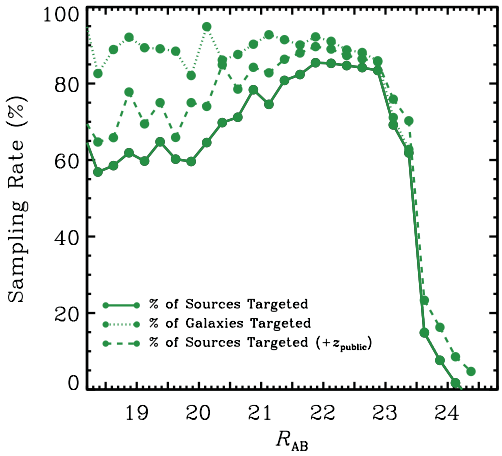

Figure 1. The ACES target sampling rate as a function of the R-band magnitude across the entire ∼30 arcmin × 30 arcmin COMBO-17/CDFS footprint. The target sampling rate is defined as the percentage of objects at a given R-band magnitude in the COMBO-17 photometric catalogue that were observed by ACES. The dotted and dashed lines show the sampling rate when only considering sources classified as non-stellar in the COMBO-17 catalogue (dotted) and when accounting for sources with a published spectroscopic redshift in the literature (dashed – see Section 2). To select the galaxy population, all sources classified as 'Star' or 'WDwarf' in the COMBO-17 photometric catalogue of Wolf et al. 2004 are excluded. At bright magnitudes, $R_{\rm AB} < 23$, ACES brings the target sampling rate in the CDFS to >80 per cent.

[1] The PRIMUS programme (Coil et al. 2011) has collected spectra for a substantial number of sources in a larger area surrounding the CDFS. However, the relatively low resolution ($R = \lambda/\Delta\lambda \sim 30$) of the prism-based spectroscopy limits the utility of the PRIMUS data set for detailed studies of spectral properties (e.g. emission-line equivalent widths) and small-scale environment (e.g. on group scales).

In addition to the main $R < 23$ target sample, we prioritized 70 μm sources detected as part of the Far-Infrared Deep Extragalactic Legacy (FIDEL) Survey (PI: M. Dickinson), which surveyed the CDFS to extremely deep flux limits at both 24 and 70 μm with *Spitzer*/MIPS (Magnelli et al. 2009, 2011). In selecting the optical counterparts to the 70 μm sources, we utilized a fainter magnitude limit of $R = 24.1$, targeting multiple optical sources in cases for which the identity of the optical counterpart was ambiguous. In total, ACES prioritized 529 sources as 70 μm counterparts, with ∼80 per cent of these sources also meeting the $R < 23$ primary magnitude limit for the survey. For the 70 μm-selected target population, our redshift success rate is quite high (∼80 per cent versus ∼70 per cent for the full target population).

As a filler population in the target-selection process, we also included (with a lower selection probability) all sources down to the secondary magnitude limit of $R < 24.1$. These fainter, optically selected sources comprise roughly 30 per cent of the total unique target sample (i.e. ∼2500 sources). The $R = 24.1$ limit was adopted to match that of the DEEP2 Survey and allows the ACES data set to probe even farther down the galaxy luminosity function at $z < 1$.

To maximize the sampling density of the survey at $0.2 < z < 1$, stellar sources were down-weighted in the target-selection process. Stars were identified according to the spectral classification of Wolf et al. (2004), which utilized template SED fits to the 17-band photometry of COMBO-17. All sources classified as 'Star' or 'WDwarf' by Wolf et al. (2004) were down-weighted in the target selection. This included a total of ∼1000 sources at $R < 23$, of which we targeted 189 obtaining secure redshifts for 162. As illustrated in Fig. 1, these stellar sources are only a significant contribution to the total R-band number counts at bright ($R < 21.5$) magnitudes; excluding this population of stars from the accounting, ACES targets >80 per cent of sources at $R < 23$.

In selecting the ACES spectroscopic targets, we also down-weighted many sources with an existing spectroscopic redshift in the literature. This sample of 'public' redshifts was drawn from Le Fèvre et al. (2004), Vanzella et al. (2005, 2006), Mignoli et al. (2005), Ravikumar et al. (2007), Szokoly et al. (2004), Popesso et al. (2009) and Balestra et al. (2010) as well as a small set of proprietary redshifts measured by the DEEP2 Galaxy Redshift Survey using Keck/DEIMOS. In all cases, only secure redshifts were employed. For example, only quality 'A' and 'B' (not 'C') redshifts were included from Vanzella et al. (2005, 2006), Popesso et al. (2009) and Balestra et al. (2010). At $R_{\rm AB} < 24.1$, a total of 2149 unique sources with a spectroscopic redshift were down-weighted in the target-selection process, with 1218 of these sources at $R < 23$. A significant number of objects (1288) in this public catalogue were observed by ACES; a comparison of the ACES redshift measurements to those previously published is presented in Section 4. Note that some of these public redshifts (most notably those of Balestra et al. 2010) were not yet published prior to the commencement of ACES, but were included in the target-selection process as the survey progressed. Also, the distribution of the existing spectroscopic redshifts on the sky is strongly biased towards the centre of the extended CDFS, primarily covering the smaller GOODS-S region (see Fig. 3).

For the 2007B through 2009B observing seasons, slitmasks were designed in pairs, sharing a common position and orientation. By placing two masks at the same location on the sky, objects had multiple chances to be included on a slitmask (and thus observed). Furthermore, we were able to integrate longer on fainter targets by including those sources on both of the masks at a given position, while only including brighter sources on a single mask and thus maximizing the number of sources observed. As will be discussed in Section 6, data for objects appearing on multiple slitmasks have yet to be combined; at present, each slitmask is analysed independently, such that there are a higher number of repeated observations of some objects (especially fainter targets).

The tiling scheme for the 40 IMACS slitmasks was designed to cover the extended ∼30 arcmin × 30 arcmin area of the extended CDFS, with the caveat that the position and orientation of each slitmask was dictated by the availability of suitably bright stars for guiding and dynamic focusing.[2] A moderate resolution grism and wide-band (5650–9200 Å) filter were employed in the observations (see Section 3), allowing multiple (two to three) targets to occupy a given spatial position on a slitmask and thereby enable upwards of ∼400 sources to be observed on a single slitmask. The average number of targets per mask was ∼350, with the details of the slitmask design varying slightly from year to year of observing.

For all of the ACES slitmasks, a standard 1 arcsec slitwidth was employed, with a minimum slitlength of ∼7 arcsec (centred on the target) and a gap of at least 0.5 arcsec between slits. For a subset of the slitmasks, slits were extended to fill otherwise unoccupied real estate on the slitmask. On every mask, the set of possible targets was restricted to those sources for which the entire spectral range of 5650–9200 Å would fall on the detector, given the position and orientation of the mask. The location of the slitmasks on the sky was selected such that the full area of the mask would fall within the CDFS region, leading to a slitmask tiling scheme that more highly samples the central portion of the field. This relative oversampling is a direct product of the large size of the IMACS field of view at $f/2$ (∼25 arcmin × 25 arcmin unvignetted); any IMACS slitmask that falls entirely within the extended CDFS region will overlap the central portion of the CDFS, independent of orientation. As shown in Fig. 2, the number of ACES slitmasks at a given position within the CDFS varies significantly from $\gtrsim$30 at the centre of the field to ∼10 at the edges.

In spite of this spatial variation in the total sampling rate, ACES achieves a relatively uniform spatial sampling rate for the main ($R < 23$) galaxy sample. As evident in Fig. 3, ACES targets $\gtrsim$80 per cent of sources at $R < 23$, relatively independent of position within the CDFS. When including spectroscopic observations from the literature (counting the associated objects as being observed), the target sampling is remarkably complete at $R < 23$, with roughly half of the ∼30 arcmin × 30 arcmin CDFS surveyed to ∼90 per cent completeness. This relatively high and uniform sampling rate is critical for the ability to measure local environments with the ACES data set.

3 OBSERVATIONS AND DATA REDUCTION

ACES spectroscopic observations employed the $f/2$ camera in the IMACS on the Magellan-Baade telescope and were completed across four separate observing seasons (2007B–2010B) as detailed in Table 1. The instrument set-up included the 200 lines mm^{-1} grism (blaze angle of 15°) in conjunction with the WB5650–9200 wide-band filter, which yields a nominal spectral coverage of 5650–9200 Å at a resolution of $R \equiv \lambda/\Delta\lambda \sim 750$ (at 7500 Å). Each slitmask was observed for a total integration time of ∼4500–7200 s, divided into (at least) three to four individual ∼1500–1800 s integrations (with no dithering performed) to facilitate the rejection of cosmic

[2] Note that the Magellan-Baade telescope includes an atmospheric dispersion corrector for the $f/11$ Nasmyth position of IMACS.

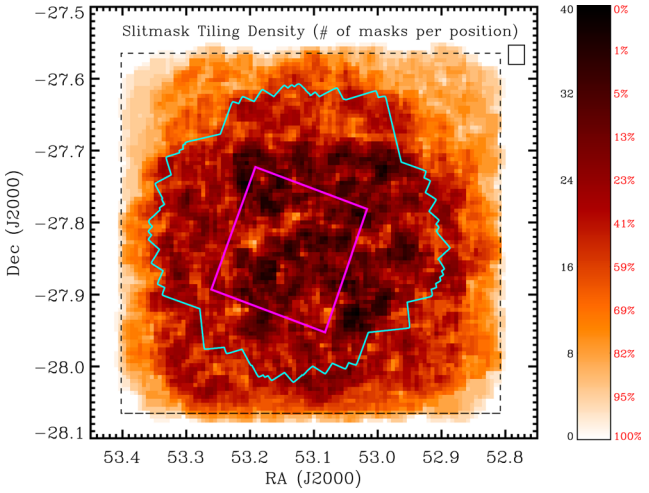

Figure 2. The number of Magellan/IMACS slitmasks covering a given spatial location (computed within a box of width $\Delta\alpha = 90$ arcsec and height $\Delta\delta = 96$ arcsec) as a function of position within the CDFS. The red values to the right of the colour bar show the portion of the 30 arcmin × 30 arcmin extended CDFS area (demarcated by the black dashed line in the plot) that is covered by more than the corresponding number of slitmasks. ACES includes a total of 40 slitmasks, with 82 per cent of the field covered by at least 8 slitmasks. Finally, the magenta and cyan outlines indicate the location of the CANDELS *HST*/WFC3-IR and 2-Ms *Chandra*/ACIS-I observations, respectively. Every object in the field has multiple chances to be placed on an ACES slitmask, helping to achieve a high sampling density and minimize any bias against objects in overdense regions on the sky.

rays – see Table 1 for details regarding the total integration times. Immediately following each set of science exposures (i.e. without moving the telescope or modifying the instrument configuration), a quartz flat-field frame and comparison arc spectrum (using He, Ar, Ne) were taken to account for instrument flexure and detector fringing.

There are two notable variations in the instrument configuration that occurred in the course of the ACES observations. Between the 2007B (2008 January) and 2008B (2008 November) observing seasons, the IMACS CCDs were upgraded from the original SITe to deep-depletion E2V chips (Dressler et al. 2011). The new CCDs provided much improved quantum efficiency, especially at red wavelengths. In addition to the detector update, for the initial observing run (2008 January), the data were collected using the incorrect grism. Instead of the 200 lines mm^{-1} grism, the higher resolution 300 lines mm^{-1} grism (blaze angle of 17°.5) was installed in IMACS. The resulting spectra from those slitmasks (ACES1–ACES8) are therefore at slightly higher resolution ($R \equiv \lambda/\Delta\lambda \sim 1100$ at 7500 Å). Given that the slitmasks multiplex in the spectral (in addition to the spatial) direction and were designed for use with the lower resolution grism, the spectra for many objects overlap significantly. In addition, for a subset of the objects (primarily those located closer to the edge of the slitmask), part of the 5650–9200 Å spectral window was dispersed off of the IMACS detector. In such instances, on the order of 300 Å was typically lost at either the blue or red extreme of the spectral window. While the data taken on this first observing run were negatively impacted by the use of the incorrect grism (including a slight reduction in total throughput), redshifts were still able to be measured for many of the targets. In an attempt to maintain the uniformity of the data set, however, the vast majority of the objects on the ACES1–ACES8 slitmasks (1166 of 1315 objects) were re-observed in subsequent observing seasons.

The IMACS spectroscopic observations were reduced using the COSMOS data reduction pipeline developed at the Carnegie Observatories (Dressler et al. 2011).[3] For each slitlet, COSMOS yields a flat-fielded and sky-subtracted, two-dimensional spectrum, with wavelength calibration performed by fitting to the arc lamp emission lines. One-dimensional spectra were extracted and redshifts were measured from the reduced spectra using additional software developed as part of the DEEP2 Galaxy Redshift Survey and adapted for use with IMACS as part of ACES and as part of the spectroscopic follow-up of the Red-Sequence Cluster Survey (RCS; Gladders & Yee 2005, *z*RCS; Yan et al. in preparation). A detailed description of the DEEP2 reduction packages (SPEC2D and SPEC1D) is presented in Cooper et al. (2012a) and Newman et al. (2012).

Example spectra for objects spanning a broad range of galaxy type and apparent magnitude are shown in Fig. 4. All spectra were visually inspected by Cooper, with a quality code (Q) assigned corresponding to the accuracy of the redshift value – $Q = -1$, 3, 4 denote secure redshifts, with $Q = -1$ corresponding to stellar sources and $Q = 3, 4$ denoting secure galaxy redshifts (see Table 2). Confirmation of multiple spectral features was generally required to assign a quality code of $Q = 3$ or 4. As discussed in Section 4.2, $Q = 3$ and 4 redshifts are estimated to be >90 and >95 per cent reliable, respectively. Quality codes of $Q = 1, 2$ are assigned to observations that yield no useful redshift information ($Q = 1$) or may possibly yield redshift information after further analysis or re-reduction of the data ($Q = 2$). For detailed descriptions of the reduction pipeline, redshift measurement code and quality assignment process refer to Wirth et al. (2004), Davis et al. (2007) and Newman et al. (2012).

4 REDSHIFT CATALOGUE

A preliminary ACES redshift catalogue is presented in Table 2, a subset of which is listed herein. The entirety of Table 2 appears in the electronic version of the journal. Note that a redshift is only included when classified as being secure ($Q = -1$, 3, 4). The total number of secure redshifts in the sample is 5080 out of 7277 total, unique targets. The redshift distribution for this sample, as shown in Fig. 5, is biased towards $z < 1$ with a tail out to higher redshift.

At bright magnitudes ($R_{AB} < 23$), ACES is highly complete, obtaining a secure redshift for $\gtrsim$60 per cent of all sources within the ∼30 arcmin × 30 arcmin COMBO-17/CDFS footprint (see Fig. 6). When excluding sources identified as stars by COMBO-17 (∼1000 sources; see Section 2) and including published spectroscopic redshifts from the literature, the redshift completeness exceeds 80 per cent at the very brightest magnitudes ($R_{AB} < 22$).

As discussed in Section 2, the ACES catalogue has a high number of repeated observations. These independent observations provide a direct means for determining the precision of the redshift measurements. As shown in Fig. 7, we find a scatter of $\sigma_z \sim 75\,km\,s^{-1}$ within the ACES sample when comparing repeat observations of a sizable sample of secure redshifts. The scatter is found to be independent of the redshift quality (i.e. $Q = 3$ versus $Q = 4$). While the precision of the ACES redshifts is poorer than that of surveys such as DEEP2 and DEEP3, it is adequate for characterizing local environments (Cooper et al. 2005) as well as identifying and measuring the velocity dispersions of galaxy groups.

[3] http://obs.carnegiescience.edu/Code/cosmos

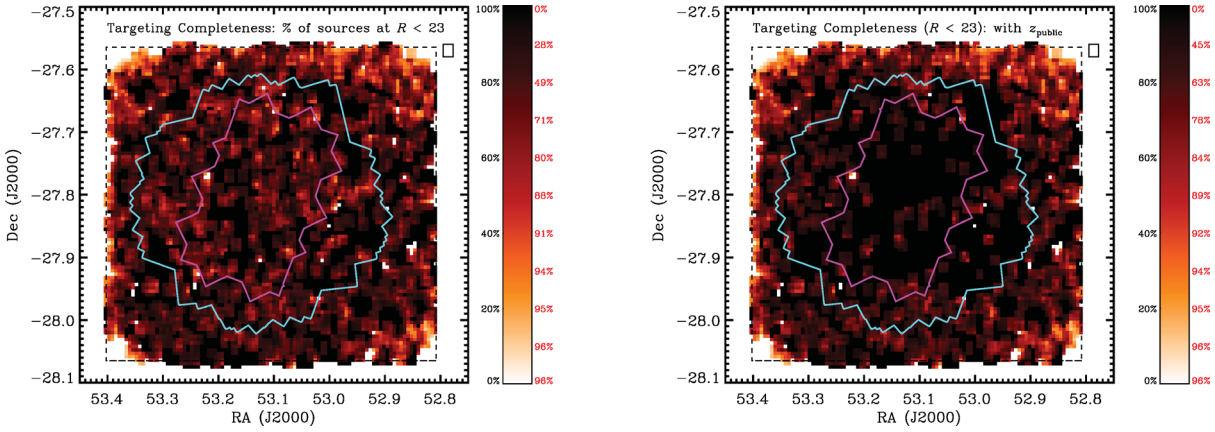

Figure 3. The target sampling rate at $R_{AB} < 23$ for the ACES target sample alone (left) and for the joint population comprised of the ACES target sample and the set of existing public redshifts detailed in Section 2 (right), computed in a sliding box of width $\Delta\alpha = 64$ arcsec and height $\Delta\delta = 72$ arcsec. The size and shape of the box are illustrated in the upper-right-hand corner of each plot. The associated colour bars give the mapping from colour to target completeness (where black and white correspond to 100 and 0 per cent completeness, respectively) and completeness is defined as the percentage of sources in the COMBO-17 imaging catalogue with $R_{AB} < 23$ (including stars) targeted by ACES (or ACES plus the set of sources with existing published redshifts). The red values to the right of each colour bar show the portion of the 30 arcmin × 30 arcmin extended CDFS area (demarcated by the black dashed line in each plot) that has a target completeness greater than the corresponding level. Finally, the magenta and cyan outlines indicate the location of the GOODS *HST*/ACS and 2-Ms *Chandra*/ACIS-I observations, respectively. At $R < 23$, the sampling rate is exceptionally high ($\gtrsim$70 per cent from ACES alone) across nearly the entire extended CDFS.

4.1 Comparison to photometric redshift samples

The ACES spectroscopic sample provides an excellent data set with which to test the precision of the COMBO-17 photometric redshift measurements. The COMBO-17 photo-z estimates are based on 17-band photometry spanning 3500 to 9300 Å. While their accuracy at higher redshift is impacted significantly by the lack of near-infrared (IR) observations, the COMBO-17 photometric redshifts are very robust at $z < 1$. Based on a comparison to a relatively small (<1000, primarily at $z < 0.3$) sample of spectroscopic redshifts, Wolf et al. (2004) found a 1σ error of $\sigma_z/(1+z) < 0.01$, with a less than 1 per cent catastrophic failure rate (where failure is defined to be $\Delta z/(1+z) > 0.05$).

In Fig. 8, we directly compare the COMBO-17 photometric redshifts to the ACES spectroscopic redshifts for all sources with a secure ($Q = -1$, 3, 4) redshift. The deficiency of objects at $z \sim 0.9$ results largely from the inability of ACES to resolve the [O II] doublet. That is, the ACES spectrum of an emission-line galaxy at $z \sim 0.9$ would yield an unresolved [O II] emission doublet at ∼7100 Å, while Hβ and [O III] would be redward of our spectral window (>9200 Å). We are unable to easily distinguish this single emission line from Hα (i.e. a galaxy at $z \sim 0.08$), as at that redshift Hβ and [O III] would be blueward of our spectral window (<5650 Å). As a result, many objects at $z \sim 0.9$ are classified as $Q = 2$. Using broad-band colour information, we hope to recover these objects in the future (e.g. Kirby et al. 2007).

Within the ACES data set alone, there are 4769 objects with a secure galaxy redshift (i.e. Q = 3,4) and a photometric redshift in the catalogue of Wolf et al. (2004). For this set of objects, the COMBO-17 photometric redshifts exhibit a dispersion of $\sigma_z/(1+z) \sim 0.015$ (with 3σ outliers removed) and a catastrophic failure rate (again taken to be $\Delta z/(1+z) > 0.05$) of >10 per cent. As highlighted by Wolf et al. (2004), however, the COMBO-17 photometric redshifts degrade in quality for increasingly fainter galaxies, and the ACES sample extends to $R = 24.1$. For bright objects ($R \leq 22$), the dispersion relative to the ACES spectroscopic redshifts is $\sigma_z/(1+z) \sim 0.012$ (again with 3σ outliers removed), with a catastrophic failure rate of 6 per cent. The precision is slightly poorer at fainter magnitudes ($22 < R < 23$), increasing to $\sigma_z/(1+z) \sim 0.014$, while at the faintest magnitudes probed by ACES, the scatter between the COMBO-17 photo-z values and our spectroscopic redshifts increases to $\sigma_z/(1+z) \sim 0.022$ (for $R \geq 23$). For the main $R < 23$ sample, the catastrophic failure rate ($\Delta z/(1+z) > 0.05$) is 8 per cent.

These trends with apparent magnitude and redshift are evident in Fig. 9, which shows the dependence of the photometric redshift error ($\sigma_z/(1+z)$) and the catastrophic failure rate on the R-band magnitude, redshift and observed $R - I$ colour based on a comparison of the ACES spectroscopic redshift and COMBO-17 photometric redshift catalogues. At faint magnitudes ($R > 23$) and at higher redshift ($z > 1$), the photometric-redshift errors and failure rates for COMBO-17 increase significantly. However, we find no significant correlation between the quality of the photometric redshifts and apparent $R - I$ colour, suggesting that there is little dependence on the spectral-type or star formation history of a galaxy.

As highlighted earlier, the degradation in photo-z quality with redshift is in part due to the lack of near-IR photometry in the multiband imaging of COMBO-17. In contrast, the photometric redshifts from the Multiwavelength Survey by Yale-Chile (MUSYC; Gawiser et al. 2006), as computed by Cardamone et al. (2010), include broad-band optical and near-IR (*JHK*) imaging in addition to photometry in 18 medium bands from Subaru. As shown in Fig. 9, the MUSYC photometric redshifts exhibit much smaller scatter in relation to the ACES spectroscopic redshift sample, with $\sigma_z/(1+z) \sim 0.005$ across the full magnitude and redshift range probed. In addition, the catastrophic failure rate for the MUSYC sample is roughly a factor of 2 lower than that found for the COMBO-17 photometric redshift catalogue.

4.2 Comparison to spectroscopic redshift samples

Matching our catalogue to previously published spectroscopic redshifts in the field (e.g. Le Fèvre et al. 2004; Vanzella et al. 2005,

Table 1. Slitmask observation information.

Slitmask name	Observation date (UT)	α (J2000)[a]	δ (J2000)[b]	P.A.[c] (deg)	N_0[d]	N_z[e]	Exposure time[f] (s)
ACES1	2008 Jan. 02	03 32 22.000	−27 53 25.00	90	376	160	7200
ACES2	2009 Jan. 02	03 32 22.000	−27 53 25.00	90	313	148	7200
ACES3	2008 Jan. 04	03 32 16.610	−27 43 58.29	90	327	168	7200
ACES4	2008 Jan. 04	03 32 16.610	−27 43 58.29	90	280	36	7200
ACES7	2008 Jan. 03	03 32 33.983	−27 54 00.00	90	339	137	7200
ACES8	2008 Jan. 03	03 32 33.983	−27 54 00.00	90	297	111	7200
ACES81	2008 Nov. 25	03 32 33.750	−27 53 48.58	90	303	170	7200
ACES82	2008 Nov. 25	03 32 33.750	−27 53 48.58	90	348	238	8631
ACES83	2008 Nov. 25	03 32 16.500	−27 54 45.00	90	343	194	7200
ACES84	2008 Nov. 26	03 32 16.500	−27 54 45.00	90	367	249	7200
ACES85	2008 Nov. 26	03 32 40.000	−27 48 30.00	0	359	273	7200
ACES86	2008 Nov. 26	03 32 40.000	−27 48 30.00	0	381	175	7400
ACES87	2008 Nov. 27	03 32 25.690	−27 49 40.00	90	376	202	7200
ACES88	2008 Nov. 27	03 32 25.690	−27 49 40.00	90	378	244	7200
ACES91	2008 Nov. 28	03 32 51.000	−27 47 45.00	0	366	212	7200
ACES92	2008 Nov. 28	03 32 51.000	−27 47 45.00	0	352	193	7200
ACES93	2008 Nov. 27	03 31 57.000	−27 47 45.00	180	364	206	7500
ACES94	2008 Nov. 28	03 31 57.000	−27 47 45.00	180	319	135	7740
ACES101	2009 Nov. 14	03 32 25.690	−27 49 40.00	90	361	172	7200
ACES102	2009 Nov. 15	03 32 25.690	−27 49 40.00	90	337	127	7200
ACES103	2009 Nov. 14	03 32 33.750	−27 53 48.58	90	345	143	9000
ACES104	2009 Nov. 14	03 32 33.750	−27 53 48.58	90	345	188	7200
ACES105	2009 Nov. 16	03 32 16.500	−27 54 45.00	90	339	132	7200
ACES106	2009 Nov. 16	03 32 16.500	−27 54 45.00	90	340	168	4800
ACES107	2009 Nov. 15	03 32 40.000	−27 48 30.00	0	348	116	6850
ACES108	2009 Nov. 15	03 32 40.000	−27 48 30.00	0	356	191	7200
ACES109	2009 Nov. 16	03 31 57.000	−27 47 45.00	180	340	127	5400
ACES110	2009 Nov. 16	03 31 57.000	−27 47 45.00	180	340	161	4500
ACES201	2010 Dec. 09	03 32 30.500	−27 49 50.00	0	370	216	4500
ACES202	2010 Dec. 10	03 32 33.750	−27 53 48.58	90	360	210	5400
ACES203	2010 Dec. 10	03 31 57.000	−27 47 45.00	180	362	243	6900
ACES204	2010 Dec. 09	03 32 40.000	−27 48 30.00	0	364	213	4500
ACES205	2010 Dec. 09	03 32 16.500	−27 54 45.00	90	352	111	4500
ACES206	2010 Dec. 09	03 32 51.000	−27 47 45.00	0	364	200	4500
ACES207	2010 Dec. 11	03 32 30.000	−27 48 00.00	90	368	227	5400
ACES208	2010 Dec. 11	03 32 25.690	−27 49 40.00	90	359	227	5400
ACES209	2010 Dec. 10	03 32 25.000	−27 46 15.00	90	361	242	5400
ACES210	2010 Dec. 10	03 32 25.690	−27 52 35.00	90	349	153	5100
ACES211	2010 Dec. 11	03 32 10.000	−27 48 00.00	0	360	210	5040
ACES212	2010 Dec. 11	03 32 54.000	−27 49 40.00	0	355	100	5400

Note – Details of the ACES Magellan/IMACS slitmasks.
[a]Right ascension (h min s) of the slitmask centre.
[b]Declination (deg arcmin arcsec) of the slitmask centre.
[c]Position angle of the slitmask (E of N).
[d]Number of targets on slitmask.
[e]Number of secure ($Q = -1, 3, 4$) redshifts measured on slitmask.
[f]Total exposure time for slitmask (s).

2006; Balestra et al. 2010, see Section 2), we find that 1288 of our targets have a redshift published as part of these existing data sets. For 941 of these 1288 objects, we measure a secure redshift from our IMACS spectroscopy. The agreement between the ACES redshifts and those in the literature is generally good. We find a median offset of $|\Delta z| \sim 240\,\mathrm{km\,s^{-1}}$ when comparing to the 'public' redshift catalogue detailed in Section 2. For the small set of significant outliers (the 44 objects with $|\Delta z| > 3000\,\mathrm{km\,s^{-1}}$), the ACES spectra were re-examined to confirm the validity of the ACES redshifts. While some outliers could be the result of mismatching between the ACES catalogue and the public data bases, the majority are the result of line misidentification (e.g. confusing Hα with [O II]) or some other failure in redshift identification (see Fig. 10).

The significant overlap between the ACES sample and the set of existing redshifts in the literature also provides a means to conservatively estimate the reliability of the ACES redshifts. Taking the previously published values to be the true redshift for each galaxy, we measure the catastrophic failure rate ($|\Delta z| = |z_{\mathrm{public}} - z_{\mathrm{ACES}}| > 1000\,\mathrm{km\,s^{-1}}$) for the $Q = 3$ and 4 ACES redshifts. For the 351 sources with $Q = 3$ and 586 sources with $Q = 4$ redshifts in the ACES catalogue, we find failure rates of 13 and 6 per cent, respectively. As shown in Fig. 10, some of the previously published redshifts are clearly in error; thus, these confidence values are

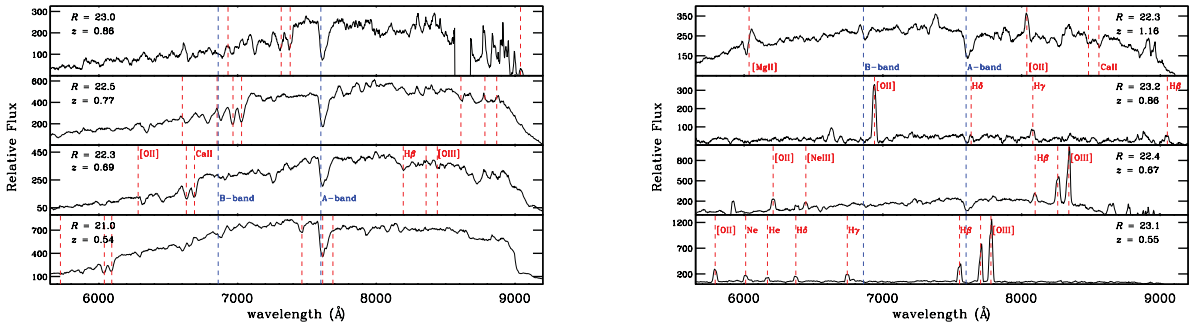

Figure 4. Example ACES one-dimensional spectra of red and/or passive galaxies (left) and star-forming/active galaxies (right). The location of prominent spectral features as well as the *A*- and *B*-band telluric features are indicated by the red and blue dashed vertical lines, respectively. Note that the spectra have been smoothed (weighted by the inverse variance) using a kernel of 15 pixels (or 30 Å) in width.

Table 2. ACES redshift catalogue.

Object ID[a]	α [b] (J2000)	δ [c] (J2000)	R_{AB} [d]	Mask[e]	Slit[f]	MJD[g]	flag$_{70\,\mu m}$ [h]	z [i]	z_{helio} [j]	Q [k]	z_{other} [l]	Ref[m]
122	53.038 740	−28.064 493	22.54	ACES105	152	551 50.9	0	0.386 87	0.386 86	4	–	–
215	53.053 105	−28.063 773	21.05	ACES106	163	551 51.7	0	–	–	1	–	–
15629	52.978 946	−27.943 812	23.15	ACES102	085	551 50.6	0	0.742 74	0.742 72	3	–	–

Note – Table 2 is presented in its entirety in the electronic edition of the journal. A portion is shown here for guidance regarding its form and content.
[a]Object identification number (SEQ) in the *R*-band catalogue of Wolf et al. (2004).
[b]Right ascension in decimal degrees from Wolf et al. (2004).
[c]Declination in decimal degrees from Wolf et al. (2004).
[d]*R*-band magnitude in the AB system from Wolf et al. (2004).
[e]Name of the IMACS slitmask on which the object was observed.
[f]Number of slit on the IMACS slitmask corresponding to the object.
[g]Modified Julian date of observation.
[h]Targeting flag: 0 = main *R*-band selected target; 1 = *Spitzer*/MIPS 70 μm target
[i]Redshift derived from the observed spectrum.
[j]Heliocentric-frame redshift.
[k]Redshift quality code (star = −1; ∼90 per cent confidence = 3; ∼95 per cent confidence = 4; unknown = 1, 2).
[l]Alternate redshift from literature.
[m]Source of alternate redshift: (1) DEEP2/DEIMOS ; (2) Le Fèvre et al. (2004); (3) Vanzella et al. (2005); (4) Vanzella et al. (2006); (5) Mignoli et al. (2005); (6) Ravikumar et al. (2007); (7) Szokoly et al. (2004); (8) Popesso et al. (2009); Balestra et al. (2010).

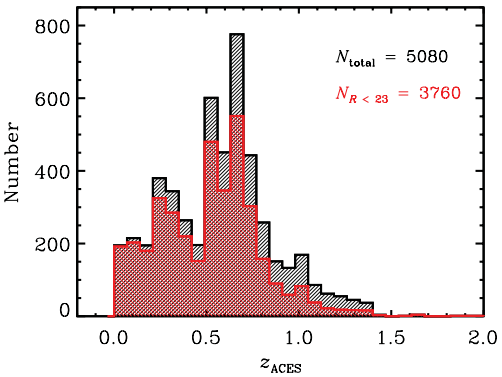

Figure 5. The distribution of the 5080 unique, secure ($Q = -1$, 3, 4) redshifts measured by ACES (black histogram). The red histogram shows the distribution for the main ($R < 23$) target sample. The main sample is biased towards $z < 0.8$, with a tail to higher redshift.

conservative estimates. Comparing within the ACES sample alone, we find that 6 and 2 per cent of sources with repeated observations (both yielding $Q = 3$ and 4 redshifts – see Fig. 7) have redshift measurements that disagree at greater than 500 km s^{-1}.

The new redshifts presented here should significantly enhance studies of galaxy evolution and cosmology in the CDFS. Our sample expands upon previous spectroscopic work in the field, significantly increasing the size of the existing redshift data base. Furthermore, our observations broaden the area covered, extending beyond the GOODS-S *HST*/ACS footprint, allowing us to target a greater number of relatively rare sources. In particular, we specifically targeted *Spitzer*/MIPS 70 μm sources, including those observed by previous spectroscopic efforts in the field. Within the FIDEL Survey's *Spitzer*/MIPS 70 μm photometric catalogue for GOODS-S, which covers an area of roughly 10 arcmin × 10 arcmin, there are only 44 sources detected at >2.5 mJy (Magnelli et al. 2011). The relatively small number of these sources puts a premium on spectroscopic follow-up, including those located outside of the GOODS-S area. The FIDEL Survey covers a broader region surrounding the GOODS-S area, actually extending significantly beyond the ACES footprint in most directions when combined with existing *Spitzer*/MIPS observations. In total, $\gtrsim$500 sources are detected (down to $S_{70\mu m} \sim 0.5$ mJy) at 70 μm within the COMBO-17 footprint as part of the FIDEL survey (requiring a 3σ detection at both 24 and 70 μm). As highlighted in Section 2, ACES targets 529 sources as potential optical counterparts to these sources (i.e. within 3 arcsec of a 70 μm source).

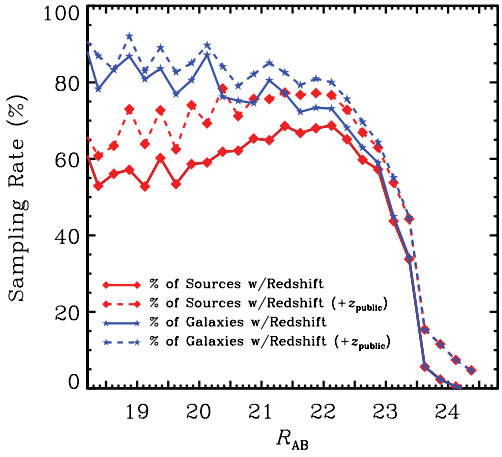

Figure 6. The ACES redshift success rate as a function of the *R*-band magnitude computed for all sources within the ∼30 arcmin × 30 arcmin COMBO-17/CDFS footprint (solid red line). The redshift success rate is defined as the percentage of objects at a given *R*-band magnitude in the COMBO-17 photometric catalogue (including stars) that were observed by ACES and yielded a secure ($Q = -1, 3, 4$ – see Section 4) redshift. The solid blue line shows the redshift completeness when only considering sources classified as non-stellar in the COMBO-17 catalogue. At bright magnitudes, $R_{AB} < 23$, the ACES sample is highly complete. The corresponding red and blue dashed lines show the associated completeness when accounting for sources with a published spectroscopic redshift in the literature (see Section 2).

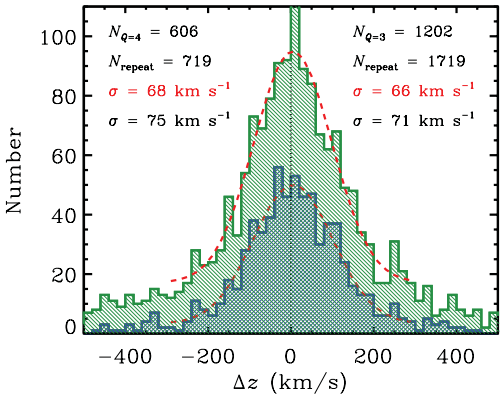

Figure 7. The distribution of velocity differences computed from repeated observations, where both observations of a given galaxy yielded a $Q = 4$ (blue histogram) or $Q = 3$ redshift (green histogram). A total of 606 and 1202 unique sources comprise the two distributions separately. The dispersions as given by a Gaussian fit to the distribution (red dashed line) and by the square root of the second moment of the distribution are reported in red and black font (or top and bottom numbers), respectively. A total of 2438 pairs of observations comprise the two distributions, with a dispersion of $\sigma \sim 75\,\mathrm{km\,s^{-1}}$ independent of redshift quality.

The 70 μm observations conducted as part of the FIDEL Survey are the deepest in the sky, allowing significant numbers of star-forming galaxies and active galactic nuclei to be detected out to intermediate redshift at rest-frame wavelengths that are dramatically less impacted by aromatic and silicate emission than those normally probed by *Spitzer*/MIPS 24 μm observations. With accompanying redshift information from spectroscopic follow-up such as presented here, these deep far-IR data provide a unique constraint on the cosmic star formation history at intermediate redshift (e.g. Magnelli et al. 2009).

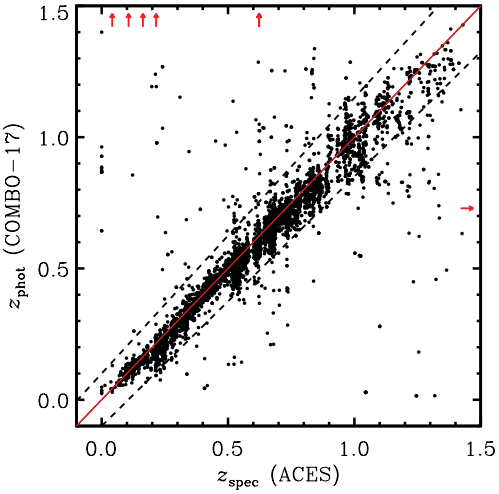

Figure 8. A comparison of the spectroscopic redshifts from ACES to the photometric redshifts of COMBO-17 (Wolf et al. 2004). In general, the agreement is quite good, with a dispersion of $\sigma_z/(1+z) \sim 0.015$ (with 3σ outliers removed) for the galaxy ($Q = 3,4$) sample. The red vertical arrows indicate sources for which the photometric redshift value is greater than $z = 1.5$, in conflict with the spectroscopic value, which is indicated by the position of the arrow (and vice versa for the red horizontal arrow). The dashed black lines correspond to a nominal catastrophic failure level of $\Delta z/(1+z) = 0.05$.

5 ENVIRONMENT MEASURES

By extending beyond the GOODS-S footprint (i.e. the area primarily targeted by previous spectroscopic efforts in the field), ACES substantially expands the area over which galaxy overdensity (or 'environment') can be measured in the CDFS. The finite area of sky covered by a survey introduces geometric distortions – or edge effects – which bias environment measures near borders (or holes) in the survey field, generally leading to an underestimate of the local overdensity (Cooper et al. 2005, 2006). To minimize the impact of these edge effects on studies of environment, galaxies near the edge of the survey field (e.g. within a projected distance of 1–2 h^{-1} comoving Mpc of an edge) are often excluded from any analysis. As such, the ACES data set, which spans a considerably larger region than previous spectroscopic samples (and with a much more spatially uniform sampling rate, see Figs 3 and 11), now allows the environment of galaxies at intermediate redshift to be accurately computed across nearly the entire ∼30 arcmin × 30 arcmin area of the CDFS, thereby enabling unique analyses of small-scale clustering in one of the most well-studied extragalactic fields in the sky.

For each galaxy in the ACES redshift catalogue (see Table 2), we estimate the local galaxy overdensity, or 'environment', using measurements of the projected third-nearest-neighbour surface density (Σ_3) about each galaxy, where the surface density depends on the projected distance to the third-nearest neighbour, $D_{p,3}$, as $\Sigma_3 = 3/(\pi D_{p,3}^2)$. Over quasi-linear regimes, the mass density and galaxy density should simply differ by a factor of the galaxy bias (Kaiser 1987). In computing Σ_3, only objects within a velocity window of $\pm 1250\,\mathrm{km\,s^{-1}}$ are counted, to exclude foreground and background galaxies along the line of sight. To explore any dependences on the choice of N in this Nth-nearest-neighbour approach to measuring environment, we also compute overdensities based on the distance to the fourth- and fifth-nearest neighbour (see Table 3).

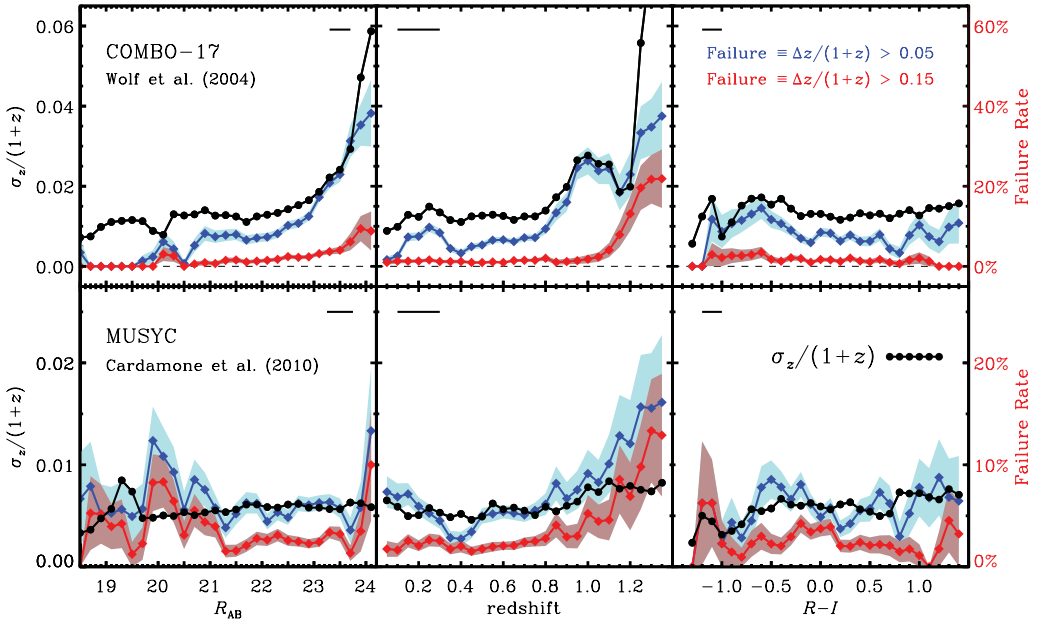

Figure 9. The dependence of the photometric redshift error ($\sigma_z/(1+z)$) and the catastrophic failure rate on the R-band magnitude (left), redshift (middle) and observed $R-I$ colour (right) for the COMBO-17 (top) and MUSYC (bottom) photometric redshift catalogues. The errors (black points) and failure rates (blue and red diamonds) are computed using sliding boxes with widths given by the black dashes in the upper corner of each plot, while the light blue and red shaded regions denote the 1σ uncertainty on the respective failure rates, as given by binomial statistics. In all cases, the dispersions ($\sigma_z/(1+z)$) are computed with 3σ outliers removed. In determining the redshift and colour dependences, only objects with $R < 23$ are included. For COMBO-17, the photo-z errors and failure rates increase significantly at fainter magnitudes ($R > 23$) and higher redshift ($z > 1$), while the trends are much weaker for the MUSYC photometric redshifts.

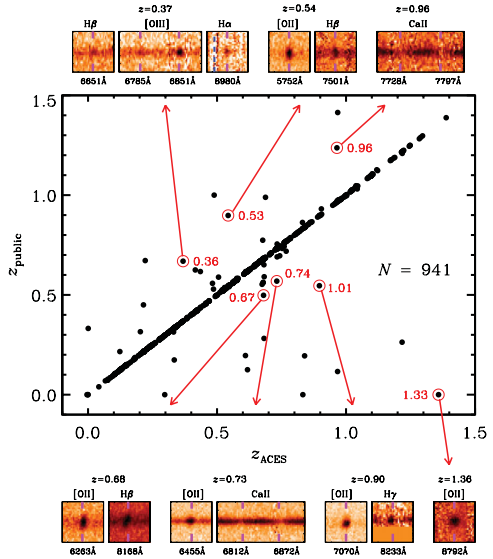

Figure 10. For the sample of 941 objects with a secure redshift in ACES (i.e. $Q = -1$, 3 or 4) and also a secure measurement in the literature, we plot a comparison of the two spectroscopic redshift measurements. The agreement is quite good, with only 47 objects having redshift measurements that disagree at $|\Delta z| > 3000\,\mathrm{km\,s^{-1}}$. For seven of these outliers, we show cut-outs from the Magellan/IMACS two-dimensional spectra, illustrating the spectral features that confirm the ACES redshift. In each case, the COMBO-17 photometric redshift (given in red font within the plot) agrees quite well with the ACES spectroscopic redshift. Refer to Section 4 for details regarding the set of 'public' redshift measurements.

When estimating the local environment within a survey data set, each surface density measurement must be corrected according to the redshift and spatial dependence of the survey's sampling rate. To minimize the variation in the spatial component of the ACES sampling rate, we select the $R < 23$ galaxy population as the tracer population by which the local galaxy density is defined – note that this is done both with and without the public redshifts included and environment measures based on each tracer population are provided in Table 3.[4] While selecting only those objects that meet this bright magnitude limit decreases the sampling density of the tracer population (relative to the full ACES data set), the main $R < 23$ galaxy sample has a well-defined and relatively uniform spatial selection rate (see Figs 3 and 11). Using this highly complete tracer population, we measure the surface density, Σ_3 (as described above), about all galaxies in the ACES redshift catalogue, independent of apparent magnitude. With or without the public redshifts included, the typical projected distance to the third-nearest neighbour, $D_{p,3}$, is $\sim 1\,h^{-1}$ Mpc at $0.2 < z < 0.8$.

To account for the relatively modest variations in completeness across the field, each surface density measure is divided by the redshift completeness at $R_{\mathrm{AB}} < 23$ (computed within a window corresponding to $1\,h^{-1}$ comoving Mpc^2 centred on each object). We define the size of the window, in this redshift-dependent manner, to roughly correspond to the typical distance to the projected third-nearest neighbour. The redshift completeness value is only weakly dependent on the size of the window employed; for example, the use of a window with fixed size (e.g. $\sim$60 arcsec or $\sim$120 arcsec on a side) yields similar results. Due to the high level of completeness achieved by ACES, the resulting correction applied to the surface density measurements is remarkably modest, with the resulting environment measures highly correlated to those computed without

[4] See Cooper, Newman & Yan (2009) and Cooper et al. (2010b) for additional discussion regarding the selection of tracer populations in the measurement of environments.

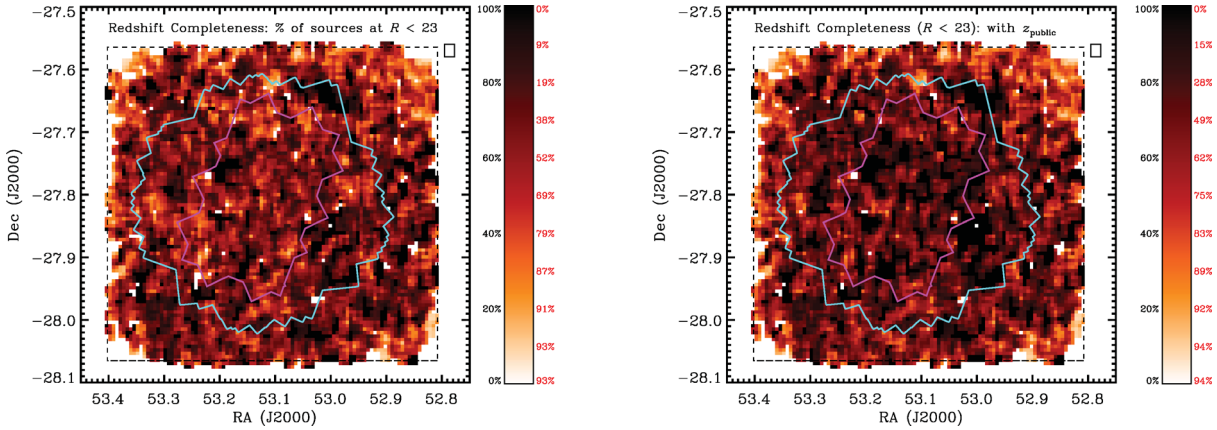

Figure 11. The redshift completeness at $R_{AB} < 23$ for the ACES sample alone (left) and for the joint population comprised of ACES and the set of existing public redshifts detailed in Section 2 (right), computed in a sliding box of width $\Delta\alpha = 64$ arcsec and height $\Delta\delta = 72$ arcsec. The size and shape of the box are illustrated in the upper-right-hand corner of each plot. The associated colour bars give the mapping from colour to redshift completeness (where black and white correspond to 100 and 0 per cent completeness, respectively) and completeness is defined as the percentage of sources in the COMBO-17 imaging catalogue with $R_{AB} < 23$ (including stars) for which ACES (or ACES plus the set of sources with existing published redshifts) measured a secure redshift (i.e. $Q = -1, 3, 4$). The red values to the right of each colour bar show the portion of the 30 arcmin × 30 arcmin extended CDFS area (demarcated by the black dashed line in each plot) that has a redshift completeness greater than the corresponding level. Finally, the magenta and cyan outlines denote the location of the GOODS *HST*/ACS and 2-Ms *Chandra*/ACIS-I observations, respectively. At $R < 23$, the redshift completeness is high ($\gtrsim$50 per cent from ACES alone) across nearly the entire extended CDFS.

Table 3. ACES environment catalogue.

Object ID[a]	z[b]	Ref[c]	D_{edge}[d]	ACES only tracer			ACES + z_{public} tracer		
				$\log(1+\delta_3)$[e]	$\log(1+\delta_4)$[f]	$\log(1+\delta_5)$[g]	$\log(1+\delta_3)$[e]	$\log(1+\delta_4)$[f]	$\log(1+\delta_5)$[g]
121	0.3164	0	0.077	−0.930	−0.768	−0.679	−0.975	−0.831	−0.731
122	0.3869	0	0.055	−0.128	0.028	0.018	−0.169	−0.050	−0.041
253	0.7689	0	0.125	−0.489	−0.313	−0.250	−0.542	−0.360	−0.305
263	0.6023	0	0.081	−1.601	−1.434	−1.416	−1.617	−1.478	−1.371

Note – Table 3 is presented in its entirety in the electronic edition of the journal. A portion is shown here for guidance regarding its form and content. Readers are reminded that galaxies located near a survey edge (e.g. within ∼1 h^{-1} comoving Mpc) should be excluded from analyses, since the associated environment measures are contaminated by edge effects (see Section 5).

[a]Object identification number (SEQ) in the *R*-band catalogue of Wolf et al. (2004).

[b]Redshift (in the heliocentric frame).

[c]Source of redshift: (0) this work; (1) DEEP2/DEIMOS ; (2) Le Fèvre et al. (2004); (3) Vanzella et al. (2005); (4) Vanzella et al. (2006); (5) Mignoli et al. (2005); (6) Ravikumar et al. (2007); (7) Szokoly et al. (2004); (8) Balestra et al. (2010).

[d]Distance from the nearest survey edge (h^{-1} comoving Mpc).

[e]Overdensity as given by the third-nearest-neighbour surface density.

[f]Overdensity as given by the fourth-nearest-neighbour surface density.

[g]Overdensity as given by the fifth-nearest-neighbour surface density.

correction for variations in redshift completeness.[5] Within the central portion of the CDFS field, the variation in redshift completeness at $R_{AB} < 23$ (including public redshifts) is well fit by a Gaussian centred at ∼0.8 (i.e. 80 per cent completeness) and with a dispersion of $\sigma < 0.1$.

To correct for the redshift dependence of the ACES sampling rate, each surface density is divided by the median Σ_3 for all galaxies within a window $\Delta z = 0.03$ centred on the redshift of each galaxy; this converts the Σ_3 values into measures of overdensity relative to the median density (given by the notation $1 + \delta_3$ herein) and effectively accounts for the redshift variations in the selection rate (Cooper et al. 2005, 2006, 2008a). We restrict our environment catalogue to the redshift range $0.2 < z < 0.8$, avoiding the low- and high-redshift tails of the ACES redshift distribution (see Fig. 5) where the variations in the survey selection rate are the greatest.

Finally, to enable the effects of edges and holes in the survey geometry to be minimized, we measure the distance to the nearest survey boundary. We determine the survey area and corresponding edges according to the two-dimensional survey completeness map ($w(\alpha, \delta)$, see Fig. 11) and the photometric bad-pixel mask, which provides information about the location of bright stars (i.e. undersampled regions) in the field. We define all regions of sky with $w(\alpha, \delta) < 0.3$ averaged over scales of $\gtrsim$30 arcsec to be unobserved and reject all significant regions of sky ($\gtrsim$30 arcsec in scale) that are incomplete in the COMBO-17 *R*-band photometric catalogue. Areas of incompleteness on scales smaller than 30 arcsec are comparable to the typical angular separation of galaxies targeted by ACES and thus cause a negligible perturbation to the measured densities. To minimize the impact of edges on the data sample, we recommend all analyses using these environment values to exclude any galaxy

[5] Estimating environment with and without applying corrections for redshift incompleteness yields overdensity measures, $\log_{10}(1 + \delta_N)$, that are highly correlated with Pearson and ranked Spearman correlation coefficients of 0.99.

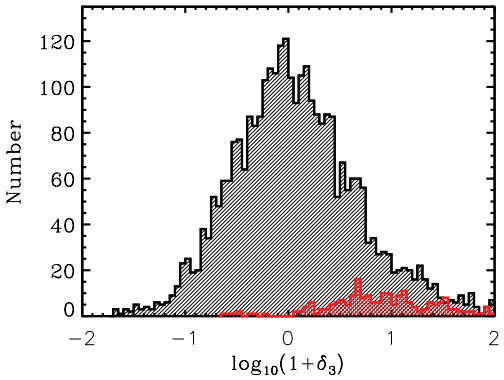

Figure 12. The distribution of overdensity measures for all sources with a secure redshift at $0.2 < z < 0.8$ in the joint population comprised of the ACES redshift catalogue and the set of existing public redshifts detailed in Section 2. The red histogram shows the environment distribution for the 210 galaxies identified as group members using the X-ray group catalogue of Finoguenov et al. (in preparation). There is good agreement between the group and environment catalogues.

within 1 h^{-1} comoving Mpc of an edge or hole; such a cut greatly reduces the portion of the data set contaminated by edge effects (Cooper et al. 2005).

In Fig. 12, we show the distribution of overdensities, $\log_{10}(1 + \delta_3)$, for 3057 galaxies with a secure redshift at $0.2 < z < 0.8$ in either the ACES redshift catalogue or the set of existing public redshifts detailed in Section 2. Here, we exclude all galaxies within $1\,h^{-1}$ comoving Mpc of a survey edge and utilize the environment measures computed with a tracer population comprised of all galaxies at $R < 23$ (using both ACES and 'public' secure redshifts). In addition, Fig. 12 shows the distribution of environments for those galaxies identified as members of X-ray groups by Finoguenov et al. (in preparation). Group members are selected within a cylinder with a radius of $0.75\ h^{-1}$ Mpc and length of $2000\,\mathrm{km\,s^{-1}}$, centred on the location of the extended X-ray emission for all groups with $M_{200} > 5 \times 10^{12}\ \mathrm{M}_{\odot}$ as given by Finoguenov et al. (in preparation), where M_{200} is the total gravitational mass (assuming $h = 0.7$) within a radius where the average density is 200 times the critical density (e.g. Finoguenov, Reiprich & Böhringer 2001). Several of the X-ray groups are coincident with known overdensities in the CDFS (e.g. Gilli et al. 2003; Adami et al. 2005; Trevese et al. 2007; Salimbeni et al. 2009), and we find that the group members are preferentially found to have higher values of $\log_{10}(1 + \delta_3)$, thereby providing an independent check of the environment measures presented here.

6 SUMMARY AND FUTURE WORK

We present a spectroscopic survey of the CDFS, conducted using Magellan/IMACS and aptly named the ACES. The survey data set includes 7277 unique spectroscopic targets, yielding 5080 secure redshifts, within the extended CDFS region. We describe in detail the design and implementation of the survey and present preliminary redshift and environment catalogues.

While this work marks a significant increase in both the spatial coverage and the sampling density of the spectroscopic observations in the CDFS, there remains much analysis of the ACES data to be completed in the future. In particular, work is presently underway to produce a relative throughput correction for the spectra, using observations of F stars that were targeted on many of the IMACS slitmasks. The F stars were observed with the same instrumental set-up as the science targets (i.e. same slitwidth, slitlength, etc.) and were included on multiple slitmasks, such that the spectra fell on each of the eight IMACS CCDs, allowing chip-to-chip variations in the throughput to be estimated.

As discussed in Section 2, fainter targets ($R \gtrsim 22.5$) were observed on multiple (approximately two to four) slitmasks, with the goal of accumulating longer integration times. In the future, these data spanning different slitmasks will be combined, which will likely improve the survey's redshift success rate at fainter magnitudes. In parallel to this work, efforts to improve the spectral reduction procedures are currently underway, which should likewise improve the redshift completeness at all magnitudes. Likewise, future work will include extracting spectra and measuring redshifts for serendipitous detections of objects, an effort that could be helped greatly by the addition of data from different slitmasks. The completion of this ongoing work is expected to coincide with a final data release, including updated redshift and environment catalogues as well as all of the reduced IMACS spectra. Finally, analysis is underway to utilize the ACES data to study the correlations between star formation history, morphology and environment at $z < 1$, using the rich multiwavelength data in the CDFS and the increased sample size to improve upon previous efforts (e.g. Capak et al. 2007; Elbaz et al. 2007; Cooper et al. 2008b, 2010a).

ACKNOWLEDGMENTS

This work is based in part on observations made with the *Spitzer* Space Telescope, which is operated by the Jet Propulsion Laboratory, California Institute of Technology under a contract with NASA. Support for this work was provided by NASA through the *Spitzer* Space Telescope Fellowship Program. MCC acknowledges support provided by NASA through Hubble Fellowship grant #HF-51269.01-A, awarded by the Space Telescope Science Institute, which is operated by the Association of Universities for Research in Astronomy, Inc., for NASA, under contract NAS 5-26555. MCC also acknowledges support from the Southern California Center for Galaxy Evolution, a multicampus research programme funded by the University of California Office of Research. This work was also supported in part by NSF grant AST-0806732 and by NASA through an award issued by JPL/Caltech as part of the FIDEL Spitzer Legacy science programme. We thank the DEEP2 Galaxy Redshift Survey team for providing access to their Keck/DEIMOS observations of the CDFS. MCC thanks John Mulchaey, Alexis Finoguenov and Dave Wilman for helpful discussions throughout much of the project and also thanks the entire Las Campanas Observatory staff for their help in the acquisition of the ACES Magellan/IMACS data. Finally, MCC thanks Mike Boylan-Kolchin for helpful discussions and the anonymous referee for valuable comments and suggestions that improved this work.

Facilities: Magellan: Baade (IMACS)

REFERENCES

Adami C. et al., 2005, A&A, 443, 805
Balestra I. et al., 2010, A&A, 512, A12
Barger A. J., Cowie L. L., Wang W., 2008, ApJ, 689, 687
Capak P. et al., 2007, ApJS, 172, 284
Cardamone C. N. et al., 2010, ApJS, 189, 270
Cohen J. G., Hogg D. W., Blandford R., Cowie L. L., Hu E., Songaila A., Shopbell P., Richberg K., 2000, ApJ, 538, 29
Coil A. L. et al., 2011, ApJ, 741, 8
Cooper M. C., Newman J. A., Madgwick D. S., Gerke B. F., Yan R., Davis M., 2005, ApJ, 634, 833

Cooper M. C. et al., 2006, MNRAS, 370, 198
Cooper M. C. et al., 2007, MNRAS, 376, 1445
Cooper M. C., Tremonti C. A., Newman J. A., Zabludoff A. I., 2008a, MNRAS, 390, 245
Cooper M. C. et al., 2008b, MNRAS, 383, 1058
Cooper M. C., Newman J. A., Yan R., 2009, ApJ, 704, 687
Cooper M. C., Gallazzi A., Newman J. A., Yan R., 2010a, MNRAS, 402, 1942
Cooper M. C. et al., 2010b, MNRAS, 409, 337
Cooper M. C. et al., 2011, ApJS, 193, 14
Cooper M. C., Newman J. A., Davis M., Finkbeiner D. P., Gerke B. F., 2012a, Astrophysics Source Code Library, record ascl:1203.003, 3003
Cooper M. C. et al., 2012b, MNRAS, 419, 3018
Cowie L. L., Barger A. J., Hu E. M., Capak P., Songaila A., 2004, AJ, 127, 3137
Damen M. et al., 2011, ApJ, 727, 1
Davis M. et al., 2003, Proc. SPIE, 4834, 161
Davis M. et al., 2007, ApJ, 660, L1
Dawson S., Stern D., Bunker A. J., Spinrad H., Dey A., 2001, AJ, 122, 598
Dickinson M. et al., 2004, ApJ, 600, L99
Doherty M., Bunker A. J., Ellis R. S., McCarthy P. J., 2005, MNRAS, 361, 525
Dressler A. et al., 2011, PASP, 123, 288
Elbaz D. et al., 2007, A&A, 468, 33
Finoguenov A., Reiprich T. H., Böhringer H., 2001, A&A, 368, 749
Gawiser E. et al., 2006, ApJS, 162, 1
Giacconi R. et al., 2001, ApJ, 551, 624
Giacconi R. et al., 2002, ApJS, 139, 369
Giavalisco M. et al., 2004, ApJ, 600, L93
Gilli R. et al., 2003, ApJ, 592, 721
Gladders M. D., Yee H. K. C., 2005, ApJS, 157, 1
Grogin N. A. et al., 2011, ApJS, 197, 35
Kaiser N., 1987, MNRAS, 227, 1
Kirby E. N., Guhathakurta P., Faber S. M., Koo D. C., Weiner B. J., Cooper M. C., 2007, ApJ, 660, 62
Koekemoer A. M. et al., 2011, ApJS, 197, 36
Le Fèvre O. et al., 2004, A&A, 428, 1043
Lehmer B. D. et al., 2005, ApJS, 161, 21
Lowenthal J. D. et al., 1997, ApJ, 481, 673
Magnelli B., Elbaz D., Chary R. R., Dickinson M., Le Borgne D., Frayer D. T., Willmer C. N. A., 2009, A&A, 496, 57
Magnelli B., Elbaz D., Chary R. R., Dickinson M., Le Borgne D., Frayer D. T., Willmer C. N. A., 2011, A&A, 528, A35
Mignoli M. et al., 2005, A&A, 437, 883
Miller N. A., Fomalont E. B., Kellermann K. I., Mainieri V., Norman C., Padovani P., Rosati P., Tozzi P., 2008, ApJS, 179, 114
Newman J. A. et al., 2012, preprint (arXiv:1203.3192)
Oke J. B., Gunn J. E., 1983, ApJ, 266, 713
Padovani P., Mainieri V., Tozzi P., Kellermann K. I., Fomalont E. B., Miller N., Rosati P., Shaver P., 2009, ApJ, 694, 235
Phillips A. C., Guzman R., Gallego J., Koo D. C., Lowenthal J. D., Vogt N. P., Faber S. M., Illingworth G. D., 1997, ApJ, 489, 543
Popesso P. et al., 2009, A&A, 494, 443
Quadri R. et al., 2007, AJ, 134, 1103
Ravikumar C. D. et al., 2007, A&A, 465, 1099
Reddy N. A., Steidel C. C., Erb D. K., Shapley A. E., Pettini M., 2006, ApJ, 653, 1004
Rix H.-W. et al., 2004, ApJS, 152, 163
Roche N. D., Dunlop J., Caputi K. I., McLure R., Willott C. J., Crampton D., 2006, MNRAS, 370, 74
Salimbeni S. et al., 2009, A&A, 501, 865
Silverman J. D. et al., 2010, ApJS, 191, 124
Szokoly G. P. et al., 2004, ApJS, 155, 271
Treu T. et al., 2005, ApJ, 633, 174
Trevese D., Castellano M., Fontana A., Giallongo E., 2007, A&A, 463, 853
Vanzella E. et al., 2005, A&A, 434, 53
Vanzella E. et al., 2006, A&A, 454, 423
Vanzella E. et al., 2008, A&A, 478, 83
Vanzella E. et al., 2009, ApJ, 695, 1163
Weiner B. J. et al., 2006, ApJ, 653, 1049
Willmer C. N. A. et al., 2006, ApJ, 647, 853
Wirth G. D. et al., 2004, AJ, 127, 3121
Wolf C., Dye S., Kleinheinrich M., Meisenheimer K., Rix H.-W., Wisotzki L., 2001, A&A, 377, 442
Wolf C. et al., 2004, A&A, 421, 913
Wolf C., Hildebrandt H., Taylor E. N., Meisenheimer K., 2008, A&A, 492, 933
Xue Y. Q. et al., 2011, ApJS, 195, 10

SUPPORTING INFORMATION

Additional Supporting Information may be found in the online version of this article:

Table 2. ACES redshift catalogue – full version.

Table 3. ACES environment catalogue – full version.

Please note: Wiley-Blackwell are not responsible for the content or functionality of any supporting materials supplied by the authors. Any queries (other than missing material) should be directed to the corresponding author for the article.

This paper has been typeset from a TEX/LATEX file prepared by the author.